Spinor self-ordering of a quantum gas in a cavity

Ronen M. Kroeze,[1,2,*] Yudan Guo,[1,2,*] Varun D. Vaidya,[1,2,3] Jonathan Keeling,[4] and Benjamin L. Lev[1,2,3]

[1]*Department of Physics, Stanford University, Stanford, CA 94305*
[2]*E. L. Ginzton Laboratory, Stanford University, Stanford, CA 94305*
[3]*Department of Applied Physics, Stanford University, Stanford, CA 94305*
[4]*SUPA, School of Physics and Astronomy, University of St Andrews, St Andrews KY16 9SS UK*

(Dated: September 24, 2018)

We observe the joint spin-spatial (spinor) self-organization of a two-component BEC strongly coupled to an optical cavity. This unusual nonequilibrium Hepp-Lieb-Dicke phase transition is driven by an off-resonant Raman transition formed from a classical pump field and the emergent quantum dynamical cavity field. This mediates a spinor-spinor interaction that, above a critical strength, simultaneously organizes opposite spinor states of the BEC on opposite checkerboard configurations of an emergent 2D lattice. The resulting spinor density-wave polariton condensate is observed by directly detecting the atomic spin and momentum state and by holographically reconstructing the phase of the emitted cavity field. The latter provides a direct measure of the spin state, and a spin-spatial domain wall is observed. The photon-mediated spin interactions demonstrated here may be engineered to create dynamical gauge fields and quantum spin glasses.

The strong interaction between quantum matter and light provided by cavity quantum electrodynamics (QED) provides unique opportunities for exploring quantum many-body physics away from equilibrium [1–3]. One particularly rich setting in which to explore such physics is provided by systems realizing the driven-dissipative (Hepp-Lieb) Dicke model of two atomic states strongly coupled to an optical cavity field [1, 3]. In this work, we present the observation of a nonequilibrium Dicke superradiant phase transition involving the spontaneous ordering of coupled atomic spin and spatial motion [4]. While previous work used atom-photon interactions to engineer spatial [5] or spin [6] self-organization, this work combines the two in a demonstration of spinor self-organization. Moreover, in this present system, cavity photons mediate an effective position-dependent spin-spin interaction; the resulting transverse Ising model that is realized opens future directions toward the study of artificial quantum spin glasses and neural networks in a driven-dissipative setting [7–16]. Moreover, with minor modification, this system could manifest dynamical gauge fields [17–22], resulting in topological superfluids and exotic quantum Hall states.

As originally proposed [23], the nonequilibrium Dicke model describes an Ising ($\mathbb{Z}_2$) symmetry-breaking transition of a spin-1/2 system coupled to a single cavity mode. The phase transition of the nonequilibrium Dicke model is closer to a classical than a quantum transition, though distinct from both [3, 24–27]. Experimentally, the nonequilibrium Dicke model could be realized by freezing the spins in a 2D lattice of period $\lambda/2$, where λ is approximately the wavelength of both the pump and cavity fields. The spins are disordered below the transition threshold and the cavity field is in a near-vacuum state. Above a pump threshold, the spins order in a λ-periodic checkerboard pattern (either up/down on the black/white sites or vice-versa) allowing the atoms to superradiantly scatter photons into the cavity mode. The emergent coherent field further orders the spins in a self-reinforcing manner. Cavity dissipation stabilizes the driven, emergent spin order, and the phase of the cavity emission locks to either 0 or π relative to the pump phase depending on the symmetry-broken state. Superradiant cavity emission of a spin-1 Dicke transition was observed with thermal atoms coupled to a cavity [6, 28].

Both pseudospin organization and superradiant emission have been observed in an alternative form of the nonequilibrium Dicke transition [5, 29, 30]. In that version, a Bose-Einstein condensate (BEC) matter wave is coupled to a cavity, where two different motional states play the role of up and down spin components. The atoms occupy either the black or white checkerboard sites (spaced λ-apart) of the emergent 2D lattice. The pseudospin organization was detected by observing Bragg peaks at a momentum consistent with a checkerboard lattice together with detection of the relative phase locking of the pump and superradiant cavity emission [5]. The organized state may be called a 'density-wave polariton condensate' in recognition of the joint light–matter-wave nature of the quasiparticles in the macroscopically occupied and coherent density-photon mode [31]. Roton instabilities and the extended Bose-Hubbard model have been realized [32–34], and similar systems employing a few degenerate cavity modes have created a supersolid [35], an intertwined spatial order [36], and supermode-density-wave polariton condensates [31]. A superradiant motional transition also occurs in cavities with spinless thermal atoms [37–39]. Self-organization of cold thermal gases and laser arrays due to optical feedback from a single mirror have also been observed [40–44].

What type of nonequilibrium phase transition arises when the pump and cavity fields couple atomic motion and spin? Reference [4] describes such a system as a nonequilibrium spin-spatial Dicke superradiant phase

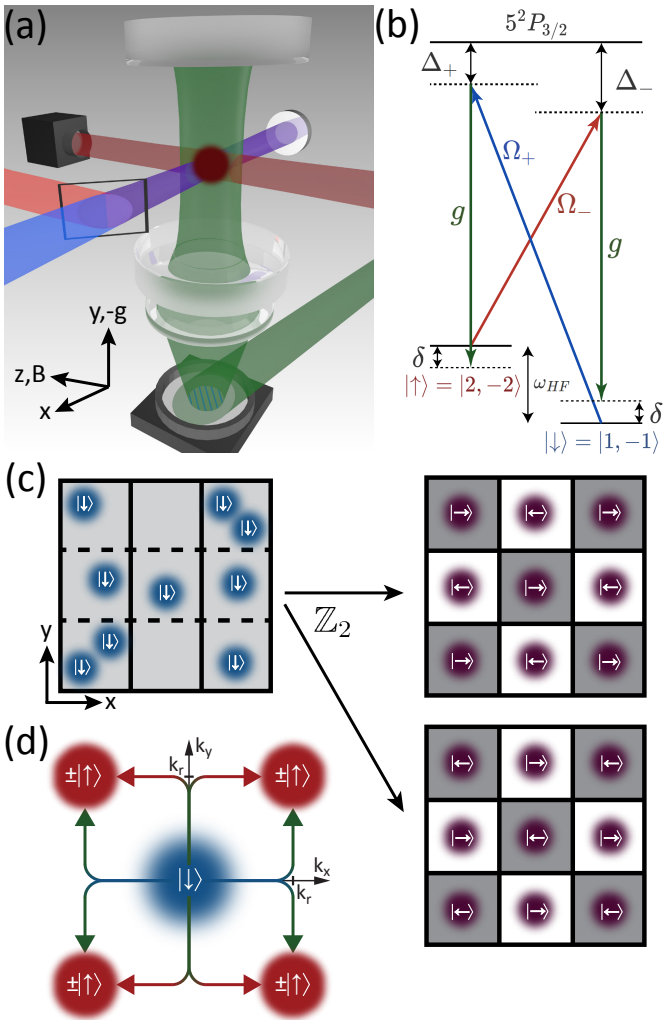

FIG. 1. (a) Experimental setup and detection techniques. The two Raman pump beams (red and blue), polarized along the cavity axis, are combined and retroreflected off the same mirror to create a phase-stable lattice (purple). The cavity mode (green), imaged onto a EMCCD camera, interferes with a local oscillator at an angle (also green). This provides the spatial heterodyne signal (blue lines) for the holographic reconstruction of the cavity field amplitude and phase. Momentum of the BEC (scarlet) is absorption-imaged in time-of-flight (scarlet beam). (b) Double Raman scheme for coupling two ^{87}Rb Zeeman states. (c) Real-space cartoon of the transition from randomly positioned atoms below threshold (left) to a checkerboard spinor order in an emergent 2D optical lattice above threshold (right panels). Atoms are in a $\hat{z}$ ($\hat{x}$) spin-polarization state below (above) threshold, where $|\leftrightarrows\rangle = |\downarrow\rangle \pm |\uparrow\rangle$. The $\mathbb{Z}_2$-order-breaking selects one of two states in which $|\rightarrow\rangle$ are at the sites colored black (right, top) or white (right, bottom). Dashed (solid) lines in left panel are the nodes of the emergent cavity (pump) field. Solid lines in the right panels are the nodes of the above-threshold 2D optical lattice. (d) Momentum-space cartoon of spin state after sequential photon recoils from the pump and cavity fields. The $|\uparrow\rangle$ spin component has phase ± 1 depending on which $\mathbb{Z}_2$ state emerges above threshold. Arrow colors depict pathway of optical transition in panel (b).

transition in which atomic spins can flip while scattering photons into the cavity, picking up recoil momentum in the process [45]. This creates a spin-decorated checkerboard lattice, whose state is a 'spinor density-wave-polariton condensate.' The spinor density wave is described by the superposition of spinor operators $\hat{\psi}_{\uparrow,\downarrow}(\mathbf{r})$ described below, and arises due to a spinor-spinor interaction proportional to $\hat{\psi}^\dagger_\uparrow(\mathbf{r}')\hat{\psi}^\dagger_\downarrow(\mathbf{r})\hat{\psi}_\downarrow(\mathbf{r}')\hat{\psi}_\uparrow(\mathbf{r})$. We note that this scenario is distinct from an emergent texture of a two-component BEC recently observed in a miscible–immiscible transition created by a state-dependent optical lattice arising from a nonequilibrium Dicke transition [46]. In this experiment, the cavity mediated a density-density interaction $\rho_{+1}(\mathbf{r})\rho_{-1}(\mathbf{r}')$ between two Zeeman states $m = \pm 1$ of a BEC and the two-component texture emerged above a critical ratio of the relative scalar and vector polarizabilities of the light fields.

We now describe the experimental system before reporting our observations of the superradiant spinor phase transition. Figure 1(a) shows the experimental configuration; see Refs. [47, 48] for details. We trap within the cavity a BEC of $4.1(3)\times10^5$ ^{87}Rb atoms in the $|F, m_F\rangle = |1,-1\rangle$ state and with Thomas-Fermi radii $(R_x, R_y, R_z) = [10.3(1), 9.4(1), 12.8(2)]$ μm. A crossed optical dipole trap confines the BEC and is formed by a pair of 1064-nm laser beams propagating along $\hat{x}$ and $\hat{z}$, resp.; its frequencies are $(\omega_x, \omega_y, \omega_z) = 2\pi\times[58(1), 63(1), 47(1)]$ Hz. These are smaller than the $w_0 = 35$ μm waist of the TEM$_{0,0}$ cavity mode [49].

To engineer the spinor Dicke Hamiltonian, we couple two internal states of ^{87}Rb, $|F, m_F\rangle = |1,-1\rangle \equiv |\downarrow\rangle$ and $|F, m_F\rangle = |2,-2\rangle \equiv |\uparrow\rangle$, through two cavity-assisted (two-photon) Raman processes; see Fig. 1(b). A bias magnetic field of $\sim$2.83 G is applied along $+\hat{z}$, the direction of the quantization axis, resulting in an energy difference $\omega_{\rm HF} \approx 6.829$ GHz between $|\uparrow\rangle$ and $|\downarrow\rangle$ due to hyperfine splitting and Zeeman shifts. The Raman processes are created by the cavity and transversely oriented pump fields. The cavity field is that of the TEM$_{0,0}$ mode at frequency ω_c with coupling strength $g = g_0\Xi(x,z)$, where g_0 is the maximum single-atom coupling rate and $\Xi(x,z)$ is the transverse mode profile. The pump beams have frequency $\omega_\pm$ such that $\omega_+ = \omega_- + 2(\omega_{\rm HF}+\delta)$, where δ is the Raman detuning. Each pump field is far detuned from the atomic excited state by $\Delta_\pm$ with coupling strengths $\Omega_\pm$. Their mean frequency $\bar{\omega} = (\omega_+ + \omega_-)/2$ is detuned by $\Delta_c = \bar{\omega} - \omega_c$ from the cavity. The pump beams are retroreflected off the same mirror to create a phase-stable lattice; see Ref. [50] for details.

This coupling realizes the interaction Hamiltonian between the two components of the spinor state $\hat{\psi}(\mathbf{r}) = [\hat{\psi}_\uparrow(\mathbf{r}), \hat{\psi}_\downarrow(\mathbf{r})]^\intercal$ given by [4, 50]:

$$H_{\rm int} = \int d\mathbf{r}\, 2\eta\hat{\sigma}_x(\mathbf{r})(\hat{a} + \hat{a}^\dagger)\cos k_r x \cos k_r y, \qquad (1)$$

where the coupling strength η is equal for both Raman transitions, $\hat{a}$ is the annihilation operator for the intra-

cavity field, and $\hat{\sigma}_x(\mathbf{r}) = [\hat{\psi}^\dagger_\uparrow(\mathbf{r})\hat{\psi}_\downarrow(\mathbf{r}) + \hat{\psi}^\dagger_\downarrow(\mathbf{r})\hat{\psi}_\uparrow(\mathbf{r})]/2$. Given the initial state $|\downarrow\rangle$, and within the single recoil scattering limit [51], the spinor components take the form $\hat{\psi}_\downarrow(\mathbf{r}) = \hat{c}_\downarrow\psi_0(\mathbf{r})$ and $\hat{\psi}_\uparrow(\mathbf{r}) = \hat{c}_\uparrow\psi_1(\mathbf{r})$, with the total atom number $N = \hat{c}^\dagger_\uparrow\hat{c}_\uparrow + \hat{c}^\dagger_\downarrow\hat{c}_\downarrow$. The zero- and one-recoil wavefunctions equal $\psi_0 = 1$ and $\psi_1(\mathbf{r}) = 2\cos k_r x \cos k_r y$, with the recoil momentum $\hbar k_r = 2\pi\hbar/\lambda$. The form of $\psi_1(\mathbf{r})$ is due to the 2D optical lattice emerging from the crossed pump and cavity standing-wave fields.

Performing the spatial integral and defining pseudospin-1/2 operators as $\hat{J}_z = [\hat{c}^\dagger_\uparrow\hat{c}_\uparrow - \hat{c}^\dagger_\downarrow\hat{c}_\downarrow]/2$ and $\hat{J}_\pm = \hat{c}^\dagger_{\uparrow\downarrow}\hat{c}_{\downarrow\uparrow}$, we arrive at the spinor Dicke-model Hamiltonian [50]:

$$H_D = -\tilde{\Delta}_c\hat{a}^\dagger\hat{a} + (2\omega_r - \tilde{\delta})\hat{J}_z + \frac{\eta_D}{\sqrt{N}}(\hat{J}_+ + \hat{J}_-)(\hat{a} + \hat{a}^\dagger). \quad (2)$$

The $\hat{\mathbf{J}}$ operate on the coupled pseudospin-1/2 spin-spatial degree of freedom. The recoil frequency is $\omega_r = \hbar k_r^2/2m$, $\tilde{\Delta}_c$ is Δ_c minus the dispersive light shift, $\tilde{\delta} = \delta - \omega_s$, where ω_s is the ac Stark shift, and $\eta_D = \sqrt{N}\eta/2$. The first two terms account for the bare cavity energy and the energy shift between the spinor pseudospin states, resp.

The organized system exhibits a nonzero order parameter $\Theta \equiv \int d\mathbf{r} \cos k_r x \cos k_r y \hat{\sigma}_x(\mathbf{r})/N$ above a critical coupling strength $\eta_D > \eta_{\rm th}$, where $\eta_{\rm th} = [\tilde{\Delta}_c(2\omega_r - \tilde{\delta})]^{1/2}/2$ and $\Theta = \pm 1$ in the $\mathbb{Z}_2$-symmetry-broken state [52]. As shown in Fig. 1(c), the organized state is one of the $|\leftrightarrows, b\rangle + |\rightleftarrows, w\rangle$ states of a spin-decorated λ-periodic checkerboard, where $|\leftrightarrows\rangle = |\downarrow\rangle \pm |\uparrow\rangle$ are the $\hat{\sigma}_x$ eigenstates and $|b/w\rangle$ are the black/white checkerboard sites. The $\mathbb{Z}_2$ broken-symmetry is reflected in the choice between $|\leftarrow\rangle$ or $|\rightarrow\rangle$ residing on black sites.

Though staggered, the spinor pseudospin state is ferromagnetic. This can be seen by integrating out the cavity field and rewriting Eq. 1 as an Ising Hamiltonian [50]:

$$H_{\rm Ising} \propto \sum J_{ij} \cos k_r x_i \cos k_r x_j \cos k_r y_i \cos k_r y_j \hat{\sigma}^i_x \hat{\sigma}^j_x. \quad (3)$$

The cosine terms can be incorporated into the $\hat{\sigma}_x$ through a local gauge rotation. This results in a ferromagnetic, infinite-range J_{ij} coupling of the locally rotated spin operators $\hat{\tilde{\sigma}}^i_x$ [50]. Figure 1(d) presents the momentum-space cartoon of the transition. Above threshold, coherent Raman scattering creates a superposition of the atoms' initial zero-momentum-$|\downarrow\rangle$ state and the $\pm|\uparrow\rangle$ state coupled to a momentum-recoil state comprised of the four superimposed $\mathbf{k} = \{(\pm k_r, \pm k_r); (\pm k_r, \mp k_r)\}$ states.

We now present the observation of this organized spinor state in momentum space. As in previous work [5, 6, 31], superradiant cavity emission heralds the nonequilibrium Dicke phase transition; see Fig. 2(a). We first demonstrate superradiance of the model by linearly increasing the power in the Raman beams through the superradiant threshold with $\Delta_c = -4$ MHz and $\delta = -10$ kHz [50].

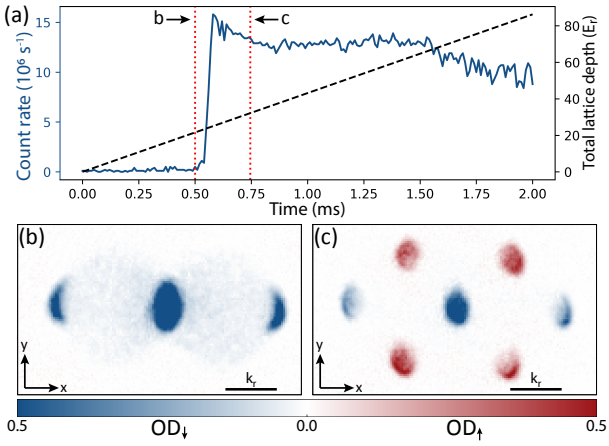

FIG. 2. (a) Cavity emission detected by single photon counters versus time plotted with the concomitant linear increase in lattice depth (proportional to pump intensity). The superradiant transition threshold is at $t \approx 0.55$ ms. (b,c) Spin-sensitive absorption images of the atomic cloud in time-of-flight reveal the optical density (OD) of the momentum distribution of both spin states at the times indicated in panel (a). (b) All atoms are in $|\downarrow\rangle$ below threshold and either at zero momentum, or at $\mathbf{k} = (\pm 2k_r, 0)$ due to pump-lattice diffraction. (c) Above threshold, atoms have undergone a spin flip to $|\uparrow\rangle$ accompanied by a $\mathbf{k} = \{(\pm k_r, \pm k_r); (\pm k_r, \mp k_r)\}$ momentum kick. The resulting Bragg peaks are spin-colored in the same pattern as in Fig. 1(d).

We then use spin-selective absorption imaging to detect the momentum distribution for each spin species independently during time-of-flight expansion of the gas. This method records the momentum of both spin components in a single realization of the experiment, allowing for observation of the spinor state associated with the spin-spatial self-ordering [50]. The spin dependent time-of-flight images are overlain in Figs. 2(b) and (c). Below threshold, Fig. 2(b) shows only $|\downarrow\rangle$, zero-momentum atoms (and Bragg peaks from the pump lattice), while above threshold, Fig. 2(c) shows that spin-decorated Bragg peaks appear in a fashion expected from Fig. 1(d). The absence of $|\uparrow\rangle$ atoms at $k = 0$ and $|\downarrow\rangle$ atoms at the 1st-order momentum peaks indicates that spinor order has emerged in the form of a λ-periodic checkerboard pattern in the $|\leftrightarrows\rangle$ basis.

Above threshold, the frequency of the superradiant cavity emission should be locked at $\bar{\omega}$ [23]. Moreover, the phase of the emission should lock to either 0 or π (depending on the $\mathbb{Z}_2$ broken-symmetry) with respect to a local oscillator (LO) field at $\omega_{\rm LO} = \bar{\omega} + \delta_{\rm LO}$. This field is coherently generated from one of the pump fields. To establish that both effects occur, we measure the phase of the cavity field emission in a spatially resolved fashion using holographic reconstruction [50]. Briefly, the LO field $E_{\rm LO}$ is shone at an angle onto the same EMCCD camera

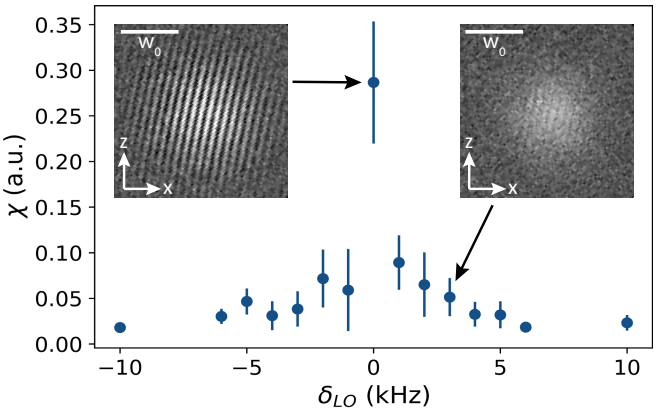

FIG. 3. Fringe amplitude factor χ as function of local oscillator frequency detuning δ_{LO}. The cavity is pumped above threshold at a detuning $\Delta_c = -4$ MHz from the $\mathrm{TEM}_{0,0}$ cavity resonance. The camera integration time is 2 ms. Insets show the spatial heterodyne signal—with local oscillator field subtracted for clarity—for both a maximal χ and where fringes average out at $\delta_{\mathrm{LO}} = 3$ kHz. Error bars represent one standard deviation over five repetitions.

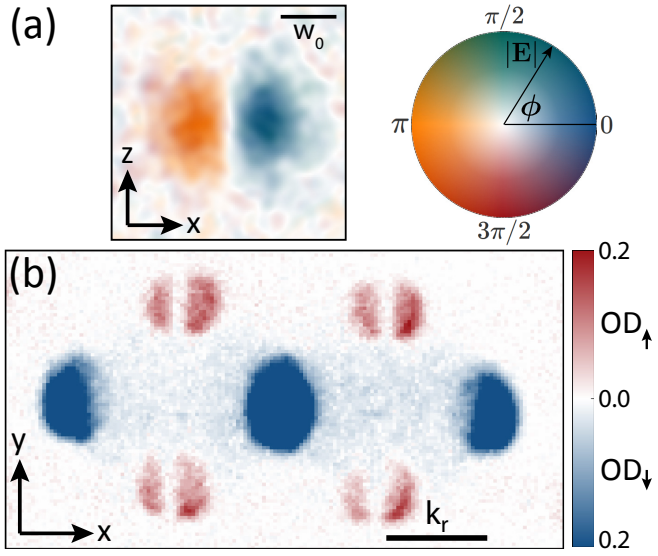

FIG. 4. (a) Holographic reconstruction of cavity field amplitude and phase for a cavity locked near the $\mathrm{TEM}_{1,0}$ mode whose spatial profile $\Xi(x, z)$ exhibits a sign-flip at $x = 0$. The phase of the right-hand lobe is defined as 0 with respect to the local oscillator. The phase shows a jump of exactly π across the cavity center, demonstrating the fixed relative phase difference between the $\Theta = \pm 1$ states with respect to the local oscillator phase. (b) Observed spin-density structure factor. The small-k transverse-mode-structure appears as a node in the 1st-order Bragg peaks. The combination of atomic and photonic observations indicates the existence of a domain wall in the spinor.

detecting the cavity emission E_c, as depicted in Fig. 1(a). If the LO has the appropriate frequency (i.e., $\delta_{\mathrm{LO}} = 0$), the phase locking between the superradiant emission and the pump beam results in spatial interference fringes on the camera, realizing a spatial heterodyne measurement of cavity field phase and amplitude [50].

The amplitude of the fringes is proportional to $\chi(\delta_{\mathrm{LO}})|E_c E_{\mathrm{LO}}|$, where the reduction of fringe contrast is characterized by the factor $\chi(\delta_{\mathrm{LO}})$ and is plotted in Fig. 3. Factors contributing to this reduction are discussed in Ref. [50]. A distinct peak appears at $\delta_{\mathrm{LO}} = 0$, as expected, while a significant averaging-out of fringe contrast is manifest for detunings larger than $1/T$, where $T = 2$ ms is the EMCCD integration time, due to a nonzero fringe phase velocity. This demonstrates a unique feature of the spinor Dicke model: cavity emission is detuned exactly halfway between the transverse pump beams, not at either or both of their frequencies. The high contrast fringes at $\delta_{\mathrm{LO}} = 0$ shows that the phase is both stable and spatially constant over the superradiant emission pattern of the $\mathrm{TEM}_{0,0}$ mode.

We now present a measurement of the relative phase locking of the cavity and pump fields. This is determined both by observing a π phase change of the superradiant emission across an induced spinor domain wall and by observing a nodal structural factor in the 1st-order atomic Bragg peaks caused by this domain wall. To create adjacent spinor domains with opposite order parameter Θ, the above experiment is repeated, but with the cavity frequency tuned near the 1st-order transverse mode $\mathrm{TEM}_{1,0}$; $\bar{\omega}$ is set to $\Delta_c = -1$ MHz [50]. The field profile $\Xi(x, z)_{1,0}$ of this mode changes sign across the $x = 0$ nodal line in the $x - z$ plane. The node appears in the superradiant cavity emission amplitude and phase are shown in Fig. 4(a). The spinor order compensates for this sign change in the cavity field by flipping the $\mathbb{Z}_2$-symmetry-broken state from $\Theta = \pm 1$ to ∓ 1 across the nodal line. That is, the spin-spatial checkerboard pattern shifts by $\lambda/2$. The system does so to allow all the atoms to superradiantly emit into the cavity in phase, thereby minimizing the organization threshold. This effect has been discussed for purely spatial organization [31].

Holographic reconstruction of the emitted cavity field reveals the existence of this π phase shift on either side of the nodal line; see Fig. 4(a). The line defect also appears in the momentum distribution of the atoms shown in Fig. 4(b). A node in the 1st-order Bragg peaks appears due to the structure factor in the spinor organization [31]. Together with the phase flip of π, the nodal structure factor implies a spinor domain wall along $(0, z)$. In degenerate-mode cavities, such as the adjustable-length near-confocal cavity system of Refs. [31, 47], interference among modes could lead to topological spin-defect textures and local spin-spin interactions [7, 48].

We have observed a spinor nonequilibrium Dicke superradiant phase transition among spinful atoms in a BEC coupled to a cavity. A domain wall in the resultant spinor density-wave polariton condensate was observed. The

photon-mediated, Ising-type spin-spin interactions realized here may enable the study of quantum spin glass physics [7, 8, 10]. Such systems may lead to quantum dissipative neuromorphic computing devices [9, 11–16]. Lastly, a simple reconfiguration of the pump fields will enable the generation of dynamical spin-orbit coupling and gauge fields [17–22].

We thank S. Goldman and K.-Y. Lin for experimental assistance and acknowledge funding support from the Army Research Office, the National Science Foundation under Grant No. CCF-1640075, and by the Semiconductor Research Corporation under Grant No. 2016-EP-2693-C. J. K. acknowledges support from SU2P.

---

* R.K. and Y.G. contributed equally to this work.

[1] H. Ritsch, P. Domokos, F. Brennecke, and T. Esslinger, "Cold atoms in cavity-generated dynamical optical potentials," Rev. Mod. Phys. **85**, 553 (2013).

[2] L. M. Sieberer, M. Buchhold, and S. Diehl, "Keldysh field theory for driven open quantum systems," Rep. Prog. Phys. **79**, 096001 (2016).

[3] P. Kirton, M. M. Roses, J. Keeling, and E. G. D. Torre, "Introduction to the Dicke model: from equilibrium to nonequilibrium, and vice versa," (2018), arXiv:1805.09828.

[4] F. Mivehvar, F. Piazza, and H. Ritsch, "Disorder-Driven Density and Spin Self-Ordering of a Bose-Einstein Condensate in a Cavity," Phys. Rev. Lett. **119**, 063602 (2017).

[5] K. Baumann, C. Guerlin, F. Brennecke, and T. Esslinger, "Dicke quantum phase transition with a superfluid gas in an optical cavity," Nature **464**, 1301 (2010).

[6] Z. Zhiqiang, C. H. Lee, R. Kumar, K. J. Arnold, S. J. Masson, A. S. Parkins, and M. D. Barrett, "Nonequilibrium phase transition in a spin-1 Dicke model," Optica **4**, 424 (2017).

[7] S. Gopalakrishnan, B. L. Lev, and P. M. Goldbart, "Frustration and Glassiness in Spin Models with Cavity-Mediated Interactions," Phys. Rev. Lett. **107**, 277201 (2011).

[8] P. Strack and S. Sachdev, "Dicke Quantum Spin Glass of Atoms and Photons," Phys. Rev. Lett. **107**, 277202 (2011).

[9] S. Gopalakrishnan, B. L. Lev, and P. M. Goldbart, "Exploring models of associative memory via cavity quantum electrodynamics," Philos. Mag. **92**, 353 (2012).

[10] M. Buchhold, P. Strack, S. Sachdev, and S. Diehl, "Dicke-model quantum spin and photon glass in optical cavities: Nonequilibrium theory and experimental signatures," Phys. Rev. A **87**, 063622 (2013).

[11] P. L. McMahon, A. Marandi, Y. Haribara, R. Hamerly, C. Langrock, S. Tamate, T. Inagaki, H. Takesue, S. Utsunomiya, K. Aihara, R. L. Byer, M. M. Fejer, H. Mabuchi, and Y. Yamamoto, "A fully-programmable 100-spin coherent Ising machine with all-to-all connections," Science **354**, 614 (2016).

[12] T. Inagaki, Y. Haribara, K. Igarashi, T. Sonobe, S. Tamate, T. Honjo, A. Marandi, P. L. McMahon, T. Umeki, K. Enbutsu, O. Tadanaga, H. Takenouchi, K. Aihara, K.-i. Kawarabayashi, K. Inoue, S. Utsunomiya, and H. Takesue, "A coherent Ising machine for 2000-node optimization problems," Science **354**, 603 (2016).

[13] V. Torggler, S. Krämer, and H. Ritsch, "Quantum annealing with ultracold atoms in a multimode optical resonator," Phys. Rev. A **95**, 032310 (2017).

[14] P. Rotondo, M. Marcuzzi, J. P. Garrahan, I. Lesanovsky, and M. Müller, "Open quantum generalisation of Hopfield neural networks," J. Phys. A: Math. Theor. **51**, 115301 (2018).

[15] E. Fiorelli, P. Rotondo, M. Marcuzzi, J. P. Garrahan, and I. Lesanovsky, "Quantum accelerated approach to the thermal state of classical spin systems with applications to pattern-retrieval in the Hopfield neural network," (2018), arXiv:1806.02747.

[16] V. Torggler, P. Aumann, H. Ritsch, and W. Lechner, "A Quantum N-Queens Solver," (2018), arXiv:1803.00735.

[17] Y. Deng, J. Cheng, H. Jing, and S. Yi, "Bose-Einstein Condensates with Cavity-Mediated Spin-Orbit Coupling," Phys. Rev. Lett. **112**, 143007 (2014).

[18] L. Dong, L. Zhou, B. Wu, B. Ramachandhran, and H. Pu, "Cavity-assisted dynamical spin-orbit coupling in cold atoms," Phys. Rev. A **89**, 011602 (2014).

[19] B. Padhi and S. Ghosh, "Spin-orbit-coupled Bose-Einstein condensates in a cavity: Route to magnetic phases through cavity transmission," Phys. Rev. A **90**, 023627 (2014).

[20] F. Mivehvar and D. L. Feder, "Synthetic spin-orbit interactions and magnetic fields in ring-cavity QED," Phys. Rev. A **89**, 013803 (2014).

[21] C. Kollath, A. Sheikhan, S. Wolff, and F. Brennecke, "Ultracold Fermions in a Cavity-Induced Artificial Magnetic Field," Phys. Rev. Lett. **116**, 060401 (2016).

[22] W. Zheng and N. R. Cooper, "Superradiance Induced Particle Flow via Dynamical Gauge Coupling," Phys. Rev. Lett. **117**, 175302 (2016).

[23] F. Dimer, B. Estienne, A. S. Parkins, and H. J. Carmichael, "Proposed realization of the Dicke-model quantum phase transition in an optical cavity QED system," Phys. Rev. A **75**, 013804 (2007).

[24] D. Nagy, G. Szirmai, and P. Domokos, "Critical exponent of a quantum-noise-driven phase transition: The open-system Dicke model," Phys. Rev. A **84**, 043637 (2011).

[25] E. G. D. Torre, S. Diehl, M. D. Lukin, S. Sachdev, and P. Strack, "Keldysh approach for nonequilibrium Phase Transitions in Quantum Optics: Beyond the Dicke model in optical cavities," Phys. Rev. A **87**, 023831 (2013).

[26] F. Piazza, P. Strack, and W. Zwerger, "Bose–Einstein condensation versus Dicke–Hepp–Lieb transition in an optical cavity," Ann. Phys. **339**, 135 (2013).

[27] S. Schütz, S. B. Jäger, and G. Morigi, "Thermodynamics and dynamics of atomic self-organization in an optical cavity," Phys. Rev. A **92**, 063808 (2015).

[28] Z. Zhang, C. H. Lee, R. Kumar, K. J. Arnold, S. J. Masson, A. L. Grimsmo, A. S. Parkins, and M. D. Barrett, "Dicke-model simulation via cavity-assisted Raman transitions," Phys. Rev. A **97**, 043858 (2018).

[29] D. Nagy, G. Kónya, G. Szirmai, and P. Domokos, "Dicke-Model Phase Transition in the Quantum Motion of a Bose-Einstein Condensate in an Optical Cavity," Phys. Rev. Lett. **104**, 130401 (2010).

[30] H. Keßler, J. Klinder, M. Wolke, and A. Hem-

merich, "Steering Matter Wave Superradiance with an Ultranarrow-Band Optical Cavity," Phys. Rev. Lett. **113**, 070404 (2014).
[31] A. J. Kollár, A. T. Papageorge, V. D. Vaidya, Y. Guo, J. Keeling, and B. L. Lev, "Supermode-density-wave-polariton condensation with a Bose-Einstein condensate in a multimode cavity," Nat. Commun. **8**, 14386 (2017).
[32] R. Mottl, F. Brennecke, K. Baumann, R. Landig, T. Donner, and T. Esslinger, "Roton-Type Mode Softening in a Quantum Gas with Cavity-Mediated Long-Range Interactions," Science **336**, 1570 (2012).
[33] J. Klinder, H. Keßler, M. R. Bakhtiari, M. Thorwart, and A. Hemmerich, "Observation of a Superradiant Mott Insulator in the Dicke-Hubbard Model," Phys. Rev. Lett. **115**, 230403 (2015).
[34] R. Landig, L. Hruby, N. Dogra, M. Landini, R. Mottl, T. Donner, and T. Esslinger, "Quantum phases from competing short- and long-range interactions in an optical lattice," Nature **532**, 476 (2016).
[35] J. Léonard, A. Morales, P. Zupancic, T. Esslinger, and T. Donner, "Supersolid formation in a quantum gas breaking a continuous translational symmetry," Nature **543**, 87 (2017).
[36] A. Morales, P. Zupancic, J. Léonard, T. Esslinger, and T. Donner, "Coupling two order parameters in a quantum gas," Nat. Mater. (2018).
[37] A. T. Black, H. W. Chan, and V. Vuletiç, "Observation of Collective Friction Forces due to Spatial Self-Organization of Atoms: From Rayleigh to Bragg Scattering," Phys. Rev. Lett. **91**, 203001 (2003).
[38] P. Domokos and H. Ritsch, "Collective Cooling and Self-Organization of Atoms in a Cavity," Phys. Rev. Lett. **89**, 253003 (2002).
[39] K. J. Arnold, M. P. Baden, and M. D. Barrett, "Self-Organization Threshold Scaling for Thermal Atoms Coupled to a Cavity," Phys. Rev. Lett. **109**, 153002 (2012).
[40] M. Nixon, E. Ronen, A. A. Friesem, and N. Davidson, "Observing Geometric Frustration with Thousands of Coupled Lasers," Phys. Rev. Lett. **110**, 184102 (2013).
[41] V. Pal, C. Tradonsky, R. Chriki, A. A. Friesem, and N. Davidson, "Observing Dissipative Topological Defects with Coupled Lasers," Phys. Rev. Lett. **119**, 013902 (2017).
[42] G. Labeyrie, E. Tesio, P. M. Gomes, G. L. Oppo, W. J. Firth, G. R. M. Robb, A. S. Arnold, R. Kaiser, and T. Ackemann, "Optomechanical self-structuring in a cold atomic gas," Nat. Photon. **8**, 321 (2014).
[43] G. R. M. Robb, E. Tesio, G. L. Oppo, W. J. Firth, T. Ackemann, and R. Bonifacio, "Quantum Threshold for Optomechanical Self-Structuring in a Bose-Einstein Condensate," Phys. Rev. Lett. **114**, 173903 (2015).
[44] G. Labeyrie, I. Kresic, G. R. M. Robb, G.-L. Oppo, R. Kaiser, and T. Ackemann, "Magnetic Phase Diagram of Light-mediated Spin Structuring in Cold Atoms," (2018), arXiv:1806.09966.
[45] See Ref. [50] for comparison to Ref. [4].
[46] M. Landini, N. Dogra, K. Kroeger, L. Hruby, T. Donner, and T. Esslinger, "Formation of a Spin Texture in a Quantum Gas Coupled to a Cavity," Phys. Rev. Lett. **120**, 223602 (2018).
[47] A. J. Kollár, A. T. Papageorge, K. Baumann, M. A. Armen, and B. L. Lev, "An adjustable-length cavity and Bose-Einstein condensate apparatus for multimode cavity QED," New J. Phys. **17**, 43012 (2015).
[48] V. D. Vaidya, Y. Guo, R. M. Kroeze, K. E. Ballantine, A. J. Kollár, J. Keeling, and B. L. Lev, "Tunable-Range, Photon-Mediated Atomic Interactions in Multimode Cavity QED," Phys. Rev. X **8**, 011002 (2018).
[49] A. E. Siegman, *Lasers* (University Science Books, 1986).
[50] See Supplemental Material [url] for information on experimental details, theory, and data analysis, which includes Refs. [54-63].
[51] Indeed, Fig. 2(c) shows that the $k = 0$ peak is much more populous than the 1st-order peaks.
[52] Evidence for $\mathbb{Z}_2$-symmetry breaking in similar superradiant transitions is in Refs. [5, 31, 37, 53].
[53] K. Baumann, R. Mottl, F. Brennecke, and T. Esslinger, "Exploring Symmetry Breaking at the Dicke Quantum Phase Transition," Phys. Rev. Lett. **107**, 140402 (2011).
[54] N. Schine, M. Chalupnik, T. Can, A. Gromov, and J. Simon, "Measuring Electromagnetic and Gravitational Responses of Photonic Landau Levels," (2018), arXiv:1802.04418.
[55] C. Emary and T. Brandes, "Chaos and the quantum phase transition in the Dicke model," Phys. Rev. E **67**, 066203 (2003).
[56] M. J. Bhaseen, J. Mayoh, B. D. Simons, and J. Keeling, "Dynamics of nonequilibrium Dicke models," Phys. Rev. A **85**, 013817 (2012).
[57] A. Altland and F. Haake, "Quantum chaos and effective thermalization," Phys. Rev. Lett. **108**, 073601 (2012).
[58] A. Altland and F. Haake, "Equilibration and macroscopic quantum fluctuations in the Dicke model," New J. Phys. **14**, 073011 (2012).
[59] F. Piazza and H. Ritsch, "Self-Ordered Limit Cycles, Chaos, and Phase Slippage with a Superfluid inside an Optical Resonator," Phys. Rev. Lett. **115**, 163601 (2015).
[60] O. Morsch and M. Oberthaler, "Dynamics of Bose-Einstein condensates in optical lattices," Rev. Mod. Phys. **78**, 179 (2006).
[61] A. Niederberger, T. Schulte, J. Wehr, M. Lewenstein, L. Sanchez-Palencia, and K. Sacha, "Disorder-Induced Order in Two-Component Bose-Einstein Condensates," Phys. Rev. Lett. **100**, 030403 (2008).
[62] J. Villain, R. Bidaux, J.-P. Carton, and R. Conte, "Order as an effect of disorder," J. Phys (Paris) **41**, 1263 (1980).
[63] A. G. Green, G. Conduit, and F. Krüger, "Quantum Order-by-Disorder in Strongly Correlated Metals," Annu. Rev. Condens. Matter Phys **9**, 59 (2018).